In Vivo Parahippocampal White Matter Pathology as a Biomarker of Disease Progression to Alzheimer's Disease

Ana Solodkin,[1,2]* E. Elinor Chen,[1] Gary W. Van Hoesen,[3] Lennart Heimer,[4] Ahmed Shereen,[1] Frithjof Kruggel,[5] and James Mastrianni[6]

[1]Department of Anatomy and Neurobiology, UC Irvine Medical School, Irvine, California 92697-3940
[2]Department of Neurology, UC Irvine Medical School, Irvine, California 92697-3940
[3]Department of Anatomy and Neurology, University of Iowa, Iowa City, Iowa 52242
[4]Department of Neurosurgery, University of Virginia, Charlottesville, Virginia 22903
[5]Biomedical Engineering, UC Irvine, Irvine, California 92697-3940
[6]Memory Center, Department of Neurology, University of Chicago, Chicago, Illinois 60637

ABSTRACT

Noninvasive diagnostic tests for Alzheimer's disease (AD) are limited. Postmortem diagnosis is based on density and distribution of neurofibrillary tangles (NFTs) and amyloid-rich neuritic plaques. In preclinical stages of AD, the cells of origin for the perforant pathway within the entorhinal cortex are among the first to display NFTs, indicating its compromise in early stages of AD. We used diffusion tensor imaging (DTI) to assess the integrity of the parahippocampal white matter in mild cognitive impairment (MCI) and AD, as a first step in developing a noninvasive tool for early diagnosis. Subjects with AD (N = 9), MCI (N = 8), or no cognitive impairment (NCI; N = 20) underwent DTI-MRI. Fractional anisotropy (FA) and mean (MD) and radial (RD) diffusivity measured from the parahippocampal white matter in AD and NCI subjects differed greatly. Discriminant analysis in the MCI cases assigned statistical membership of 38% of MCI subjects to the AD group. Preliminary data 1 year later showed that all MCI cases assigned to the AD group either met the diagnostic criteria for probable AD or showed significant cognitive decline. Voxelwise analysis in the parahippocampal white matter revealed a progressive change in the DTI patterns in MCI and AD subjects: whereas converted MCI cases showed structural changes restricted to the anterior portions of this region, in AD the pathology was generalized along the entire anterior–posterior axis. The use of DTI for in vivo assessment of the parahippocampal white matter may be useful for identifying individuals with MCI at highest risk for conversion to AD and for assessing disease progression. J. Comp. Neurol. 521:4300–4317, 2013.

INDEXING TERMS: DTI; microstructure; MCI; AD conversion; limbic; perforant pathway

The development of noninvasive biomarkers for Alzheimer's disease (AD) pathology is essential to improve premorbid diagnostic accuracy and to monitor the effectiveness of therapies as they are developed. The postmortem diagnosis of AD is based on the presence, density, and distribution of two hallmark features; neurofibrillary tangles (NFTs) and amyloid-rich neuritic plaques (Gomez-Isla et al., 2008; Trojanowski, 2002; Wippold et al., 2008). Ideally, biomarkers should therefore target these histopathological hallmarks. Currently, positron emission tomography (PET) studies can identify amyloid plaques (Clark et al., 2012; Driscoll et al., 2012; Furumoto et al., 2013; Okamura and Yanai, 2010; Ono, 2009), but NFTs have been less well studied (Braskie et al., 2010; Jensen et al., 2011; Shin et al., 2011; Small et al., 2002).

Several reports agree that accumulation of NFTs signals neuronal death and that their distribution and density correlate highly with disease severity (Gomez-Isla et al., 1996). In AD, the cortical region that displays the

Grant sponsor: Brain Research Foundation; Grant sponsor: James McDonnell Foundation; Grant number: JSMF22002082 (to A.S.).

*CORRESPONDENCE TO: Ana Solodkin, PhD, Department of Anatomy and Neurobiology and Neurology, UC Irvine School of Medicine, Hewett Hall, Room 1505, Irvine, CA 92697-3940. E-mail: solodkin@uci.edu

Received March 14, 2013; Revised June 14, 2013;
Accepted June 19, 2013.
DOI 10.1002/cne.23418
Published online July 10, 2013 in Wiley Online Library (wileyonlinelibrary.com)

highest number of NFTs is the entorhinal cortex (EC) within the ventromedial temporal lobe (Van Hoesen et al., 1991), where NFTs make up a high percentage of the large multipolar neurons that form layer II of the EC in AD (Van Hoesen and Solodkin, 1993). The critical nature of these changes is best appreciated by considering the connectional relation between the hippocampus and the rest of the cerebral cortex. The EC gives rise to the perforant pathway, a major neural system of the temporal lobe, which terminates on the hippocampus. This pathway represents the greatest source of cortical input to the hippocampus and represents a key link to the remainder of the cortex (Duvernoy, 1988; Rosene and Van Hoesen, 1977). Importantly, in the preclinical stages of AD, the cells of origin for the perforant pathway, in layers II and III of the EC, in addition to the neurons of the perirhinal cortex, are the first to display NFTs (Braak and Braak, 1997b). Hence, it is expected that their presence should affect the axons of the perforant pathway and then the cell bodies of layers II and III (Van Hoesen et al., 2000).

Based on the hierarchical and temporal distribution of NFTs that develops over the course of AD, several imaging techniques have been applied to assist in making an early diagnosis. The most important of these are magnetic resonance imaging (MRI) methods, including 1) T1-weighted MRI to assess the degree of atrophy in specific limbic regions or to identify specific AD-like atrophy patterns [SPARE-AD (Davatzikos et al., 2009, 2010; Misra et al., 2009)] and 2) MR spectroscopy to measure neuronal metabolites (for reviews see Chetelat et al., 2005; De Toledo-Morrell et al., 2000; Hampel et al., 2008; Jack et al., 2010; Small, 2002; Sprooten et al., 2009). However, because these approaches are likely to require a significant degree of neuronal death before showing alterations, a more sensitive method that detects subtle changes in tissue integrity prior to neuronal death is necessary. A third MRI method, diffusion tensor imaging (DTI), permits the assessment of microstructural characteristics of specific brain pathways (Basser and Pierpaoli, 1996; Filler and Bell, 1992; Le Bihan et al., 2001; Pierpaoli et al., 1996). This method has already shown significant utility in the assessment of cerebral ischemia, acute stroke, multiple sclerosis, and traumatic brain injury (de Crespigny et al., 1995). Several studies have already used DTI to assess the integrity of hippocampal white matter pathways in AD, whether alone (Fellgiebel et al., 2004; Muller et al., 2005) or in combination with hippocampal atrophy (Arenaza-Urquijo et al., 2010; Bosch et al., 2010; Chen et al., 2009; Cherubini et al., 2010; Damoiseaux et al., 2009; Fellgiebel et al., 2006; Liu et al., 2009; Muller et al., 2005; Sexton et al., 2010; Stenset et al., 2009; Teipel et al., 2010). However, it has not yet been possible to make individual predictions on which subjects with MCI have the highest likelihood of converting to AD.

As a first step toward the development of a sensitive, noninvasive technique for the preclinical diagnosis of AD, we tested whether DTI MRI could be used to detect a disruption of white matter integrity in an area that includes the perforant pathway. Furthermore, we evaluated this technique for its potential to predict which subjects with mild cognitive impairment (MCI) would convert to AD early. MCI is a diagnosis that carries a high risk for conversion to AD within the subsequent 3–5 years (Modrego, 2006; Petersen, 2004; Petersen and Negash, 2008), but only a fraction of those diagnosed, ranging from 10% to 50% (Geslani et al., 2005; Petersen, 2004), will convert at all. It is currently impossible to predict, based on noninvasive testing alone, who will convert and who will not. In fact, it has been reported retrospectively that MCI subjects who eventually convert to AD tend to have lower fractional anisotropy (FA) and higher mean diffusivity (MD) values in several brain regions at initial assessment (Fellgiebel et al., 2006; Kalus et al., 2006; Rose et al., 2006). Others have found that patients with MCI show a correlation between cognitive impairment and a decrease in FA or MD in the perforant pathway region (Kalus et al., 2006; Rogalski et al., 2009). However, such group analyses do not provide predictive probabilities for individuals with MCI, i.e., the ability to determine at the time of initial evaluation the risk that a single individual will convert to AD. In the current study, we investigated the use of DTI measures as potential predictors of risk of progression from MCI to AD for individual patients. By expanding beyond group differences, we aimed to develop a real-world application of the technique. The goal of this study was to determine whether DTI measurements within the ventromedial temporal lobe differ between control and AD subjects and, if so, whether altered measures in MCI can potentially predict the risk for future conversion to AD.

MATERIALS AND METHODS

Subjects

Research volunteers were prospectively and consecutively recruited from the Center for Comprehensive Care and Research on Memory Disorders at The University of Chicago. Control subjects were recruited from within the local community or were caregivers of patients. Individuals with pre-existing severe psychiatric or neurological illness (e.g., cerebrovascular disease or evidence of stroke on brain imaging) or dementia other

than AD were excluded. The diagnosis of probable AD followed the recommendations of the joint working group of the NINCDS and the AD and Related Disorders Association (NINCDS-ADRDA; McKhann et al., 2011). Specific diagnoses for each individual were developed at a consensus conference comprising neurologists, neuropsychologists, social workers, and geriatricians. If the Folstein Mini-Mental State Exam (MMSE) score was 26 or higher, all subtest scores of the neuropsychological battery were less than 1.0 standard deviation below normal, and there were no impairments in activities of daily living (ADLs) or instrumental activities of daily living (iADLs), the subject was labeled as "no cognitive impairment" (NCI). The diagnostic criteria for MCI were modeled after those used in the Memory Impairment Study (Albert et al., 2011) and included 1) memory complaint by patient or informant; 2) abnormal memory function, documented by scores greater than 1 SD from the mean on delayed recall in the Hopkins Verbal Learning Test; 3) no impairments in ADLs or iADLs; 4) normal general cognitive function; and 5) not sufficiently impaired, cognitively or functionally, to meet NINCDS-ADRDA criteria for AD. All MCI cases enrolled were labeled "amnestic MCI," because memory impairment was the predominant cognitive feature, and none had significant cerebrovascular disease on imaging to suggest a vascular component, the major diagnostic category predicted by multidomain MCI.

One year later, MCI subjects were reassessed by the same clinicians, who were blind to the initial predictions obtained from the imaging data. This study and all procedures for recruitment and consent were approved by the Institutional Review Board of the Division of Biological Sciences of The University of Chicago. All participants or their proxy gave written consent for their participation in the study.

Neuropsychological assessment

Neuropsychological assessments were administered by a trained psychometrist and included the Wide Range Achievement Test–III (Wilkinson, 1993), Mini-Mental State Examination or MMSE, Trail Making Test (Reitan, 1958), Clock Drawing Test (Spreen and Strauss, 1998), Boston Naming Test (Kaplan et al., 1983), Controlled Oral Word Association Test & Category Fluency (Spreen and Strauss, 1998), Hopkins Verbal Learning Test–Revised (Shapiro et al., 1999), Brief Visual Spatial Memory Test–Revised (Benedict et al., 1996), and Geriatric Depression Scale (Yesavage et al., 1983).

Imaging procedures

Scanning was performed on a clinical 3T GE Signa MRI scanner (GE, Waukesha, WI) equipped with high-strength gradients. The following sequences were used in all subjects. 1) For high-resolution anatomical imaging, the 3D magnetization-prepared rapid acquisition gradient echo (MP-RAGE) was TE = 3.2 msec, TR = 8 msec, preparation time = 725 msec, flip angle 6°, field of view 24 cm × 24 cm, 124 sagittal slices, 1.5 mm slice thickness, 192 × 256 image matrix reconstructed to 256 × 256, scan time: 9 minutes 58 seconds; 2) For DTI using Turboprop-DTI, TR = 3,500 msec, 8 spin-echoes per TR (ETL = 8), 5k-space lines per spin echo (turbo-factor = 5; thus each blade contained 8 × 5 = 40 lines), 16k-space blades per image, field of view = 24 cm × 24 cm, 25 contiguous oblique coronal slices, and 3 mm slice thickness, and all images were reconstructed to a 256 × 256 matrix; DW images with b = 900 seconds/mm^2 were acquired for a set of 12 diffusion directions; two b = 0 seconds/mm^2 images were also acquired, and scan duration was 13 minutes 3 seconds; 3) proton density (PD) fast spin echo (FSE) sequence with two echo times provided PD and T2-weighted images in the same slice locations as the Turboprop-DTI: TE_1 = 20 msec, TE_2 = 117 msec, TR = 7,000 msec, ETL = 16, field of view = 24 cm × 24 cm, 25 contiguous oblique coronal slices, 3 mm slice thickness, 192 × 256 image matrix reconstructed to 256 × 256; images from both echo times were collected twice and averaged to improve signal to noise (NEX = 2), and scan duration was 5 minutes 36 seconds.

Primary image analysis

The mismatch produced by motion between DTI volumes was corrected by registering each of the 12 diffusion-weighted image and the PD volumes to the mean diffusion-weighted volume using the automated image registration algorithm (AIR; Woods et al., 1998). FA, MD, axial diffusivity ($\lambda 1$), and radial diffusivity (RD; Pierpaoli et al., 1996) maps were produced for each hemisphere in regions of interest (ROIs) using the FMRIB Diffusion Toolbox (Behrens et al., 2003).

ROIs

ROIs were manually outlined in the PD images (guided by the higher resolution of the MP-RAGE images to detect finer details) and used as masks on the DTI images for quantification of the DTI metrics in the specified regions, as in other systems (Solodkin et al., 2004). These regions were manually outlined using known landmarks (Van Hoesen, 1995), as recently confirmed with a DTI sequence in humans (Augustinack et al., 2010; Zeineh et al., 2012): 1) parahippocampal white matter region defined anteriorly by a vertical plane at the level of the middle portion of the amygdala and the rhinal sulcus, if present (corresponding to the anterior limit of the EC); posteriorly by the vertical

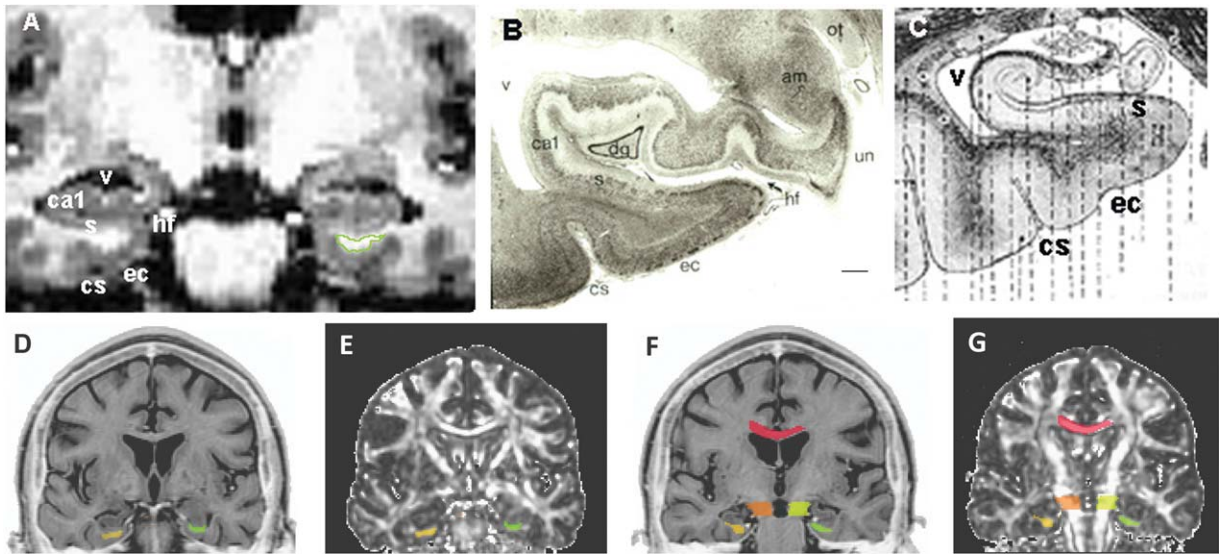

Figure 1. Coronal sections depicting the location and landmarks of the parahippocampal white at the level of the entorhinal region. **A:** T1-weighed MRI. **B:** Nissl-stained section. As depicted by Dejerine and Dejerine-Klumpke (1901; **C**) and in the MPRAGE (**D,F**) and DTI (**E,G**) images. The white matter ROI containing the parahippocampal white region is highlighted in A in green so that the reader can compare its location to the landmarks used. The MPRAGE was chosen for presentation clarity purposes only since the actual ROIs were drawn in the PD images obtained with similar resolution to the DTI. The Nissl-stained section shows the main landmarks and neighboring regions limiting the entorhinal and hippocampal regions. Note that, in the graphic representation of the hippocampal region by Dejerine and Dejerine-Klumpke (1901), the fibers of the perforant pathway are shown penetrating the subiculum. The lower row shows samples of the actual ROIs as seen in an anterior and a posterior slice of the entorhinal area. ec, Entorhinal cortex; hf, hippocampal fissure; cs, collateral sulcus; dg, dentate gyrus; s, subicular complex; am, amygdalar body; un, uncus of the hippocampus; ot, optic tract. Scale bar = 2 mm.

plane at the level of the lateral geniculate; and laterally by the collateral sulcus. Figure 1 shows a coronal section at the level of the anterior entorhinal cortex, depicting the mask used to determine the region of the parahippocampal white matter. 2) The cerebral peduncle (CP) was used as a reference measure, because primary sensory and motor cortices are among the last cortical regions to develop NFTs in AD (Arnold et al., 1991; Suva et al., 1999). It was defined at the level of the midbrain, with the posterior limit demarcated by the substantia nigra. ROIs (performed by a neuroanatomist, A.So.) were traced twice. The reproducibility of the regions (rater blinded to the first measurement) was demonstrated by the 97% spatial overlap between the two tracings. The photomicrograph (Fig. 1B) was obtained by high-resolution scanning of the original film (HP Scanjet 5500c) and stored using Photoshop, in which the contrast was increased (+3). The generation of DTI metrics and ROIs was performed blind to the clinical status of the subjects.

Statistical analysis

Comparing mean values to subdivide the MCI group

To determine the conversion of MCI cases to AD, we performed statistical analysis at the group level based on mean DTI values. For this, the first step was to establish group differences between the AD and the NCI groups. To assess simultaneously the differences between groups across the two hemispheres, we first performed a Shapiro-Wilks test to determine multivariate normality for each measure (FA, MD, $\lambda 1$, and RD) for the parahippocampal white matter and CP vectors. Box's M-test was used to assess whether the AD and NCI groups had similar covariance matrices, and, if so, a parametric multivariate Hotelling T^2 test was used to assess the two hemispheres simultaneously. Otherwise, the nonparametric Cramer test was used.

Discriminant analysis

Discriminant analysis was performed to obtain additional segregation among the mean FA, MD, $\lambda 1$, and RD values in the parahippocampal white matter of AD and NCI groups and was conducted in two steps. First, the Wilks lambda test was used to guarantee that the discriminant function successfully separated the two groups. Second, we used the "leave-one-out" (or cross-validation) method to estimate correct classification rates. In this process, each individual case with a known membership was taken out from the group, and its membership was reassigned based on the remaining cases. Correct classification rate was expressed as the

proportion of correctly reassigned cases from the total cases in each group.

Numerous studies have suggested that the yearly rate of conversion from MCI to AD is between 10% and 15% and up to 50% after 5 years (Buchanan, 2009; Butts et al., 2011; Fischer et al., 2007; Lehrner et al., 2005; Petersen, 2004). Consequently, we expected that our MCI group would display a large variance in the DTI data. To avoid this confound inherent in a group statistical analysis, we compared individual MCI subjects with the AD and NCI groups. We first assumed an equal probability of each DTI metric from each MCI subject to belong to either the AD or the NCI group. We then assigned each measure to the corresponding group through the quantification of the smallest Mahalanobis distance. This computation refers to the distance in mean FA, MD, $\lambda 1$, and RD values between each subject and the centroid of the AD and NCI groups. This analysis provided a way to predict the MCI individuals most likely to progress to AD. Finally, to assess possible confounds with partial tissue volumes, we calculated Pearson's correlation within groups, between FA values and the volume of the parahippocampal white matter region.

Computing finer resolution on the structural architecture of the parahippocampal white matter

To associate white matter changes with potential structural features in the parahippocampal white matter, we performed statistical analysis at the individual voxel level. DTI metrics were extracted on a voxel-by-voxel basis from the parahippocampal ROIs, and their frequency distributions were calculated. Differences of skewness between AD and NCI were determined for each DTI metric using the Cramer test, and comparisons on the distributions were performed with the Kolmogorov-Smirnov test.

Clustering analysis centered on the FA/MD distributions was used to determine contrasts between groups, and clusters were modeled based on a multivariate Gaussian distribution (mclust software; Fraley and Raftery, 2007). Clusters represented by ellipsoids of variable size, shape, and orientation were selected based on a Bayesian Information Criterion (Schwarz, 1978). Using the mean values from the cluster with the highest FA and lowest MD values (derived from the NCI group) as a reference origin, we calculated the Mahalanobis distances to this origin for all voxels from each group. Differences between groups were obtained using the Wilcoxon signed-rank test and corrected for multiple comparisons with the Westfall-Young procedure. Finally, the mean values of these distances were mapped back to the anatomical space in the anterior–posterior axis of the parahippocampal ROI. All statistical evaluations were performed in SPSS 13.0 for Windows and R 2.1.1 software.

RESULTS

Patient groups

In total 37 subjects were enrolled. Nine subjects met criteria for AD, 19 were labeled as NCI, and nine met criteria for MCI. The mean age of subjects was 75 (range 64–89) years for the NCI group, 78 (66–89) years for the AD group, and 79 (67–91) years for the MCI group. The Mini-Mental State Exam (MMSE) scores were significantly lower in the AD group (mean 20.2, range 12–25) compared with the NCI (mean 27.7, range 26–30) and MCI (mean 28.6, range 25–29) groups, although the latter two groups did not differ statistically from each other. Because one of the MCI subjects presented structural MRI abnormalities in the entorhinal cortex, this subject was excluded from the study. The demographics of our cohorts are detailed in Table 1.

DTI

Values for the four DTI metrics (FA, MD, $\lambda 1$, RD) are listed in Table 2, and Figure 2 shows individual examples in the anatomical space. In contrast to the measurements within the parahippocampal white matter region, the DTI metrics values in the cerebral peduncles for AD and NCI were highly consistent (Table 2).

Group analysis

Normality of mean distributions assessed by the Shapiro-Wilks test and their resultant probability values are listed in Table 3. Except for the FA in the parahippocampal white matter of the AD group, all metrics had normal and close-to-normal distributions. Box's M-test indicated that the AD and NCI groups did not have similar covariance matrices for FA, MD, $\lambda 1$, and RD values in either ROI, except for the FA in the CP ($P = 0.24$). Therefore, quadratic discriminant analysis was used.

Group comparisons

The Cramer nonparametric test confirmed a highly significant difference of FA in the parahippocampal white matter region between the NCI and the AD groups ($P = 1.0 \times 10^{-3}$). The Hotelling T^2 tests showed highly significant differences of MD ($P = 2.04 \times 10^{-4}$), $\lambda 1$ ($P = 0.0167$), and RD ($P = 2.78 \times 10^{-4}$) as well (Fig. 3). In contrast, no significant differences in FA ($P = 0.45$), MD ($P = 0.38$), $\lambda 1$ ($P = 0.10$), or RD ($P = 0.66$) were found in the CP between these two groups.

Pearson's correlation

Correlation between averaged FA values and the volumes of the parahippocampal white matter region were not

TABLE 1.

Neuropsychological Raw Scores Defining the Cognitive Profile for the AD and MCI Subjects[1]

Patient No.	Diagnosis	Age (years)	Education	MMSE	WRAT3 reading	HVLT delayed memory	BVMT delayed memory	Trails A	Trails B time	BNT	COWAT	Category	GDS	Clock drawing
1	AD	73	14	21	94	0	0	56	221	19	28	8	11	2
2	AD	72	16	19	105	0	1	48	300	42	25	11	0	4
3	AD	80	20	25	112	0	2	39	125	44	22	18	4	8
4	AD	76	14	19	99	0	2	117	300	26	11	8	11	2
5	AD	66	3	19	96	0	0	54	300	43	11	5	18	2
6	AD	81	12	23	87	0	3	55	300	11	18	5	2	8
7	AD	87	10	18	91	0	0	54	300	32	20	10	2	2
8	AD	90	14	12	87	1	1	96	300	23	8	2	5	10
9	AD	75	8	21	72	0	0	125	300	18	4	9	2	6
10	MCI	80	12	28	98	0	6	36	193	43	17	8	13	8
				30	96	5	7	53	141	39	25	10	13	8
11	MCI	71	13	29	103	3	8	36	115	44	41	15	3	10
12	MCI	77	14	28	113	7	8	38	98	58	52	21	8	
				30	*117*	*6*	*0*	*44*	*74*	*58*	*50*	*28*	*9*	*6*
13	MCI	75	16	29	112	0	3	40	118	51	39	20	11	6
				29	*115*	*0*	*4*	*46*	*168*	*48*	*42*	*22*	*12*	*8*
14	MCI[2]	91	16	25	106	0	4	33	99	31	44	13	6	8
				20	*100*	*0*	*0*	*42*	*236*	*35*	*48*	*10*	*2*	*8*
15	MCI[2]	81	16	27	113	0	5	84	118	55	51	13	4	8
				25	*111*	*1*	*4*	*87*	*97*	*56*	*38*	*9*	*3*	*8*
16	MCI	75	18	29	118	6	10	45	110	59	42	16	3	10
				29	*118*	*6*	*10*	*45*	*110*	*59*	*51*	*16*	*3*	*8*
17	MCI[2]	82	16	25	98	3	5	57	277	38	26	11	8	10
				24	*89*	*3*	*0*	*65*	*300*	*43*	*18*	*13*	*6*	*10*

[1]The cells under every MCI case with italics depict the retesting of the MCI subjects 1 year later. The shaded cells mark the scales showing decline at posttest. MMSE, Mini-Mental State Examination; score out of 30; WRAT, Wide Range Achievement Test–III; standard scores are reported for more meaningful interpretation; HVLT, Hopkins Verbal Learning Test–revised; score out of 12; BVMT, Brief Visual Spatial Memory Test–revised; score out of 12; Trails A and B, Trail Making Test (time in seconds); BNT, Boston Naming Test; score out of 60; COWAT, Controlled Oral Word Association Test; Category, Category Fluency (number of words produced); GDS, Geriatric Depression Scale; score out of 20.
[2]MCI patients considered to have declined since their scores worsened in more than two subtests of the neuropsychological battery.

TABLE 2.

Summary of DTI Metrics in the Two Patient Groups and in Controls

ROI	Group	FA ± SD	MD ± SD (mm^2/second)	λ1 ± SD (mm^2/second)	RD ± SD (mm^2/second)
Parahippocampal	NCI	0.3760 ± 0.0398	8.39E−04 ± 3.61E−05	1.23E−03 ± 8.03E−05	7.76E−04 ± 1.85E−04
	MCI	0.3714 ± 0.1121	9.04E−04 ± 1.34E−04	1.27E−03 ± 1.35E−04	7.22E−04 ± 1.66E−04
	AD	0.3085 ± 0.0766	1.03E−03 ± 1.55E−04	1.34E−03 ± 1.42E−04	9.41E−04 ± 1.85E−04
Cerebral peduncle	NCI	0.5442 ± 0.0392	9.60E−04 ± 6.21E−05	1.57E−03 ± 7.59E−05	6.54E−04 ± 6.85E−05
	MCI	0.5505 ± 0.0825	1.06E−03 ± 2.05E−04	1.73E−03 ± 2.04E−04	7.22E−04 ± 2.29E−04
	AD	0.5631 ± 0.0545	1.02E−03 ± 1.70E−04	1.67E−03 ± 1.89E−04	6.94E−04 ± 1.67E−04

significant. For the AD group, r = −0.09, $P = 0.72$ (t-test = −0.367; DF = 16); for the MCI group, r = 0.42, $P = 0.08$ (t-test = 1.87; DF = 16); and, for the NCI group, r = 0.41, $P = 0.050$ (t-test = 2.14; DF = 36).

Suitability of discriminant analysis

Besides the obvious group differences between the NCI and the AD groups, probability values calculated by the Wilks lambda test suggested that the groups could be separated based on any of the four DTI metrics obtained from the parahippocampal white matter region. Furthermore, the cross-validation tests showed a correct classification rate for the FA values in this region of 79% for the NCI group and 67% for the AD group; MD 84% and 67%, λ1 84% and 67%, and RD 95% and 78%. Table 4 summarizes these results.

Classification of individual MCI cases as either AD or NCI

From the eight MCI subjects tested, three (38%) were assigned membership to the AD group, and five were assigned to the NCI group. Table 5 shows the predicted

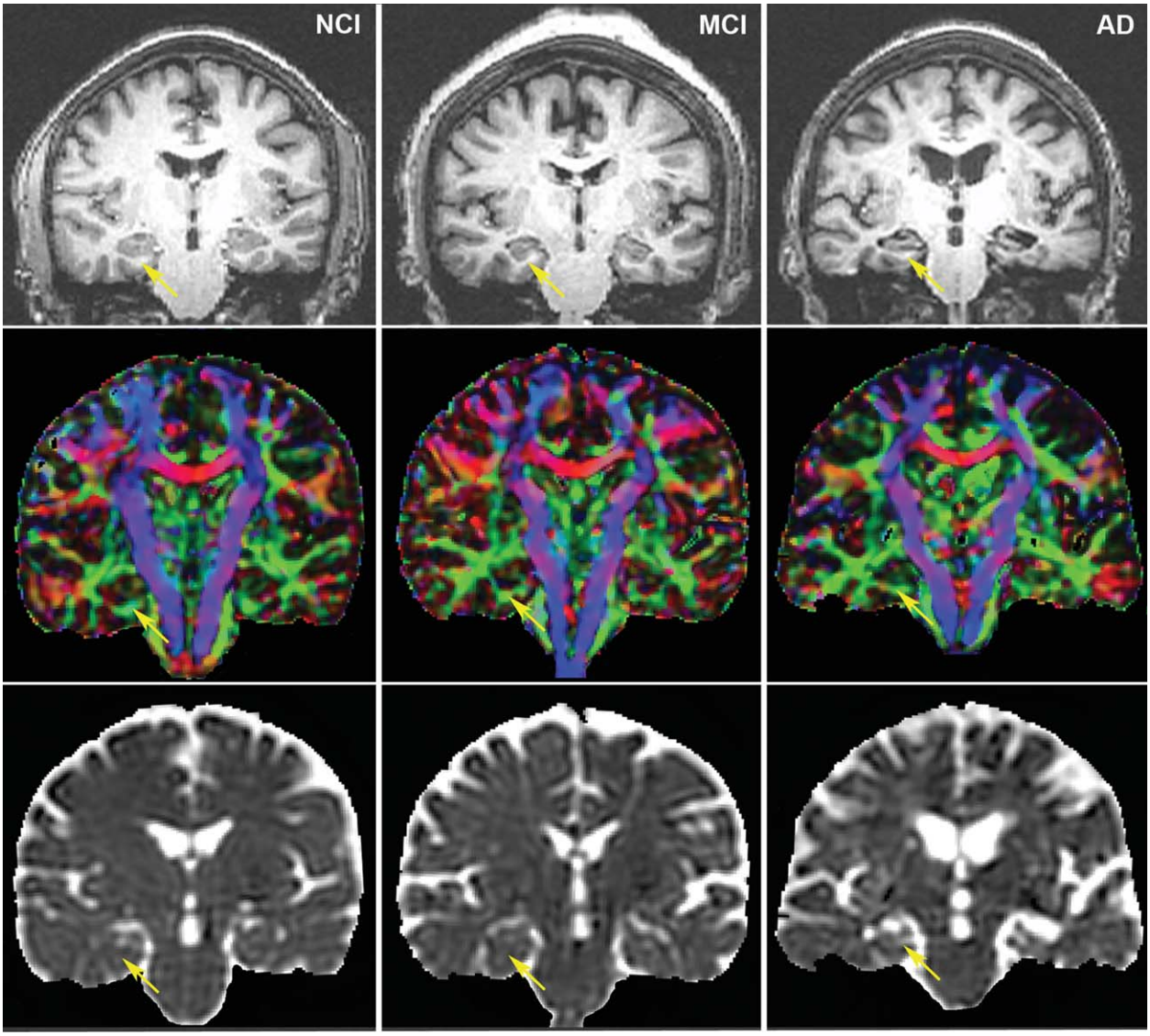

Figure 2. Individual examples of structural MRI images depicting the white matter in the parahippocampal region. *Left column*: control subject. **Middle column:** MCI subject. **Right column:** Alzheimer's disease subject. The first row of images depicts coronal T1-weighted images obtained from the MPRAGE sequence. Note the significant degree of atrophy, reflected by the enlargement of the lateral ventricles and sulci, present in the Alzheimer's disease subject. The second row of images represents the directionally encoded FA color maps obtained in the oblique-coronal plane in the same subjects. The red color indicates a left-to-right direction; blue, superior to inferior; green, front to back. Note the decrease in the intensity of the signal in the AD subject compared with control. The third row of images depicts the mean diffusivity maps obtained in the oblique-coronal plane. Arrows point to the location of the parahippocampal white matter region in the right hemispheres.

group and the associated probability values obtained for each MCI patient who participated in the study. Note that all four DTI metrics resulted in identical membership predictions for the large majority of the subjects (the only exception occurred in two MCI [NCI] cases, for whom three-fourths of the metrics were in agreement).

MCI conversions to AD after 1 year

All MCI patients underwent a detailed neuropsychological battery and a reassessment of their functional abilities 1 year from the initial assessment. The clinical examiners were blinded as to each subject's original DTI classification. Among the three MCI subjects originally classified as AD (14, 15, and 17), two definitely fulfilled criteria for probable AD, and the third demonstrated significant cognitive decline by neuropsychological assessment. Whereas subjects 14 and 17 had documented evidence of ADL or iADL impairment and, as such, met full criteria for probable AD, subject 15 did not report ADL or iADL problems. Despite this, the clinical team labeled this patient as "probable early AD"

based on the overall decline (particularly in verbal and visual tasks), and the questionable report of intact ADLs. Therefore, this subject was started on anticholinesterase therapy. The specific assessment data for each subject are listed in Table 1. An asterisk identifies those that progressed. Among the five MCI subjects classified as NCI by DTI, none was diagnosed as AD on followup, and all continued to meet MCI criteria.

TABLE 3.

Assessment of Multivariate Normality: Probability Values Resulting From the Shapiro-Wilks Test for the NCI and AD Groups

Pathway	Metrics	NCI	AD
Parahippocampal	FA	0.190	0.003
	MD	0.783	0.529
	λ1	0.100	0.480
	RD	0.226	0.508
Corticospinal	FA	0.128	0.413
	MD	0.391	0.035
	λ1	0.730	0.593
	RD	0.132	0.060

Voxelwise analysis

Frequency distributions

The distribution of the total number of voxels from the AD or the NCI group showed a fair amount of overlap on all DTI metrics (Fig. 4). However, except for axial diffusivity, the other three distributions from the AD group were shifted to either the left (FA) or right (MD and RD). Comparisons of the skewness (Cramer test) between the NCI and AD groups showed significant differences for FA ($P = 0.002$) but not MD ($P = 0.052$),

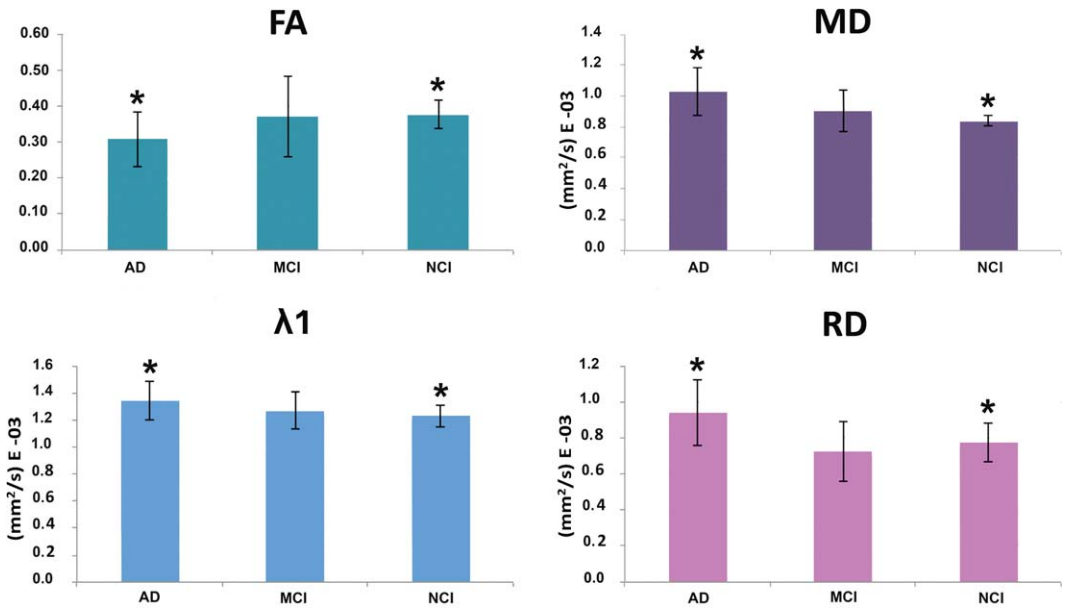

Figure 3. Graphic representation of the mean DTI metrics in NCI, MCI, and AD. Panels show mean values for each DTI metrics (FA, MD, λ1, and RD) with their corresponding standard deviations in each of our cohorts. Clear progressive trends toward AD were noted, as seen with a decrease in FA and an increase in λ1, MD, and RD. For each metric displayed, the variance of the MCI group was larger than that in either the AD or the NCI groups. Significant differences between groups are represented by asterisks.

TABLE 4.

Summary Values for Discriminant Analysis Performed on the DTI Metrics in AD and NCI Groups in the Parahippocampal White Matter[1]

	ROI	FA	MD	λ1	RD
Box's M-test(*P*)	Parahippocampal	0.01	9.12E−05	5.49E−03	2.32E−06
	CP	0.24	2.86E−04	8.33E−04	2.52E−03
Wilks' λ (*P*)	Parahippocampal	0.0022	0.0002	0.0167	0.0003
	CP	0.4478	0.3835	0.1049	0.6621
Cross-validation(%)	AD	67	67	67	78
	NCI	79	84	84	95

[1]Box M-tests equality of variance, Wilks lambda assesses success of separation between groups and cross validation measures accuracy of classification.

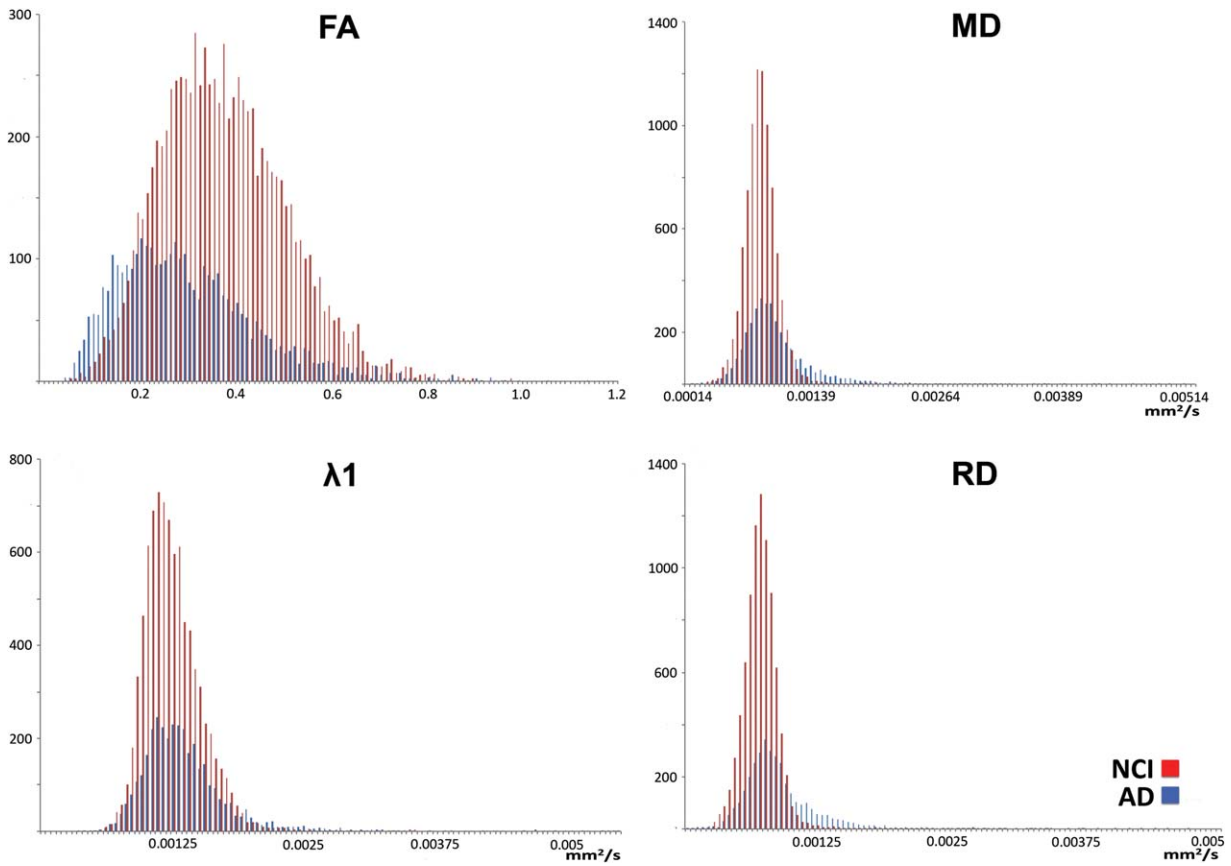

Figure 4. Voxelwise analysis. Comparing frequency distributions of DTI metrics in the NCI and the AD groups. Panels represent the distribution of FA, MD, λ1, and RD for all voxels in the NCI group (red bars) and the AD group (blue bars). Note the partial overlap of the distributions for all except the axial diffusivity, for which the overlap is complete.

TABLE 5.

Statistical Classification of Individual MCI Cases Into Either the AD or the NCI Groups[1]

	FA		MD		λ1		RD	
MCI subjects	Group	*P*	Group	*P*	Group	*P*	Group	*P*
1	NCI	0.95	NCI	0.80	NCI	0.75	NCI	0.81
2	NCI	0.72	NCI	0.92	NCI	0.94	NCI	0.93
3	NCI	0.82	NCI	0.71	NCI	0.74	NCI	0.86
4[2]	AD	0.65	AD	0.82	AD	0.88	AD	0.90
5	NCI	0.92	NCI	0.68	AD	0.80	NCI	0.92
6[2]	AD	0.86	AD	0.99	AD	1.00	AD	1.00
7	AD	0.52	NCI	0.90	NCI	0.91	NCI	0.83
8[2]	AD	0.86	AD	0.57	AD	0.98	AD	1.00

[1]The columns reflect the group assigned and the probability value associated with it for each DTI metric.
[2]MCI patients considered to have declined by clinical criteria 1 year later.

RD ($P = 0.027$), or λ1 ($P = 0.141$) after applying Bonferroni's corrections for multiple comparisons. These results did not depend on voxel number, because distributions (Kolmogorov-Smirnov test) between the NCI and AD groups still showed highly significant differences for FA, MD, RD, and λ1 ($P < 10^{-11}$). To obtain a better discrimination among voxels, we also determined their distribution in two-dimensional space: FA-MD and λ1-RD. In these cases, the distributions differed between the AD and the NCI groups for FA-MD ($P = 0.02$) but not for λ1-RD ($P = 0.03$). Based on the fact that significance was limited to the FA-MD space, cluster analysis was performed based on this distribution alone. Figure 5 shows these distributions and those for the two MCI groups (nonconverters and converters). Note that the graph representing the MCI groups shows a topology reminiscent of the corresponding topology found in the graphs for the AD-NCI groups.

Cluster analysis

Cluster analysis detected segregation of voxels into clusters within each cohort. That is, voxels in each group had membership in either one of two clusters. As Figure 6 illustrates, there was a cluster (purple dots in

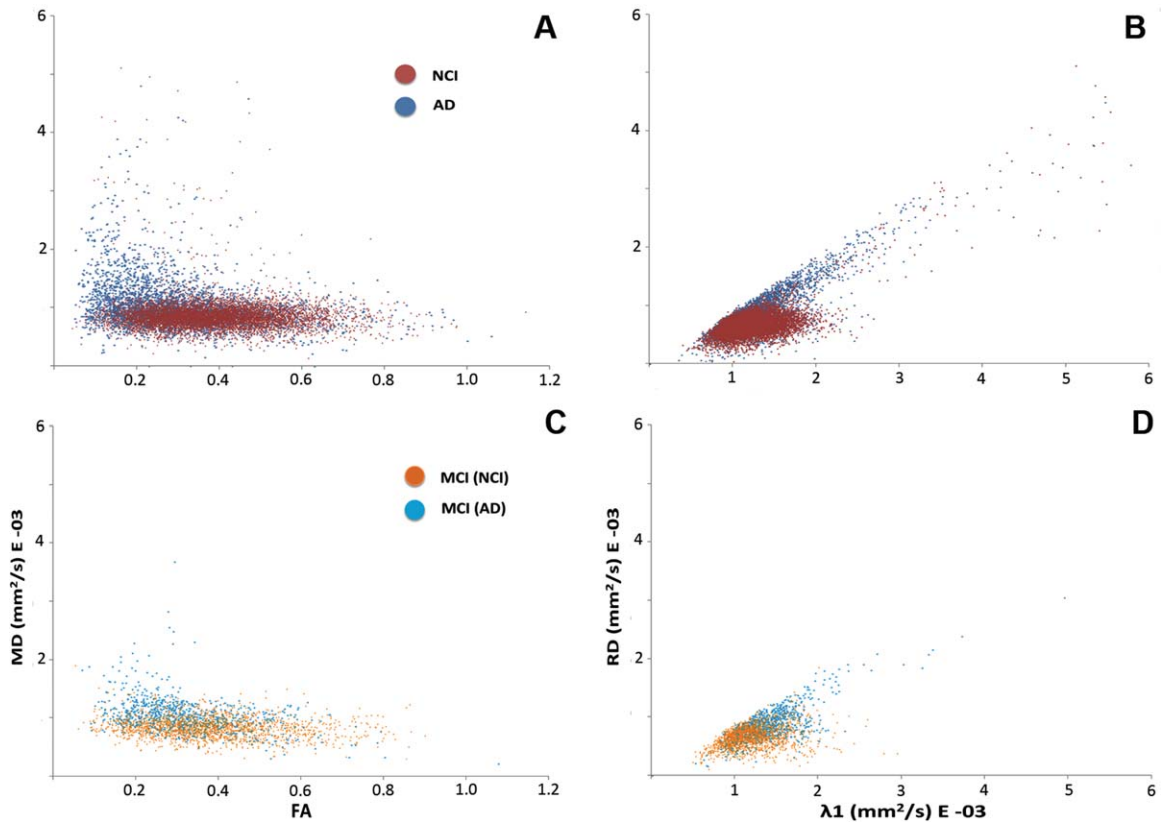

Figure 5. Multivariate scatterplots for FA-MD and λ1-RD. Upper panels represent voxel distribution in the FA-MD (**A**) and the λ1-RD (**B**) space for the NCI (red dots) and the AD (blue dots) groups. In both distributions, voxels from the AD group separate from those in controls at low FA and high MD values (in A) and for high RD values (in B). **C** and **D** represent similar representations but for the converted MCI (MCI [AD]) in turquoise dots and the nonconverted MCI [MCI(NCI)] in orange dots. Their distributions, although in smaller scale, are reminiscent of those shown in the panels above.

Fig. 6) common to the thrtee groups representing metrics in the high FA (center of mass around 0.4–0.5) and low MD (0.001 mm^2/second) values. Because of this commonality, we considered the cluster derived from the NCI group as the reference origin, representing voxels with the largest structural integrity. Figure 6 also illustrates the existence of an additional population of voxels in the NCI, MCI, and AD groups (marked green) that have different locations with respect to the reference cluster. That is, some are closer to the reference and some are farther. These voxels had different locations in each group. Hence, whereas in controls they are close to the reference, in the MCI group they are clearly segregated, with many values shifted to a lower FA range, highlighting the larger variance of this group. These differences are further evolved in the AD group, among whom a more pronounced shift toward lower FA values is accompanied by higher MD values. This produces larger distances among these voxels with respect to the reference.

Mahalanobis distances from the reference cluster

Statistical differences of FA/MD distances in relation to the reference cluster showed that, whereas in controls and MCI (NCI) these distances are independent of location in the anatomical space, early changes (larger distances in MCI [AD] compared with NCI) start in the anterior portion of the parahippocampal region ($P = 10^{-5}$ after correction for multiple comparisons). By contrast, later changes seen as larger distances in AD compared with MCI (AD) affect the posterior portion of the parahippocampal white matter ($P = 10^{-5}$ after correction for multiple comparisons; Fig. 7). These observations show that properties of voxels deviate from the reference cluster in NCI to MCI (AD) and then to AD, starting in the anterior parahippocampal white matter in MCI (AD) and extending subsequently to the posterior portion in AD. These changes cannot be attributed to size, because the cross-sectional area (number of

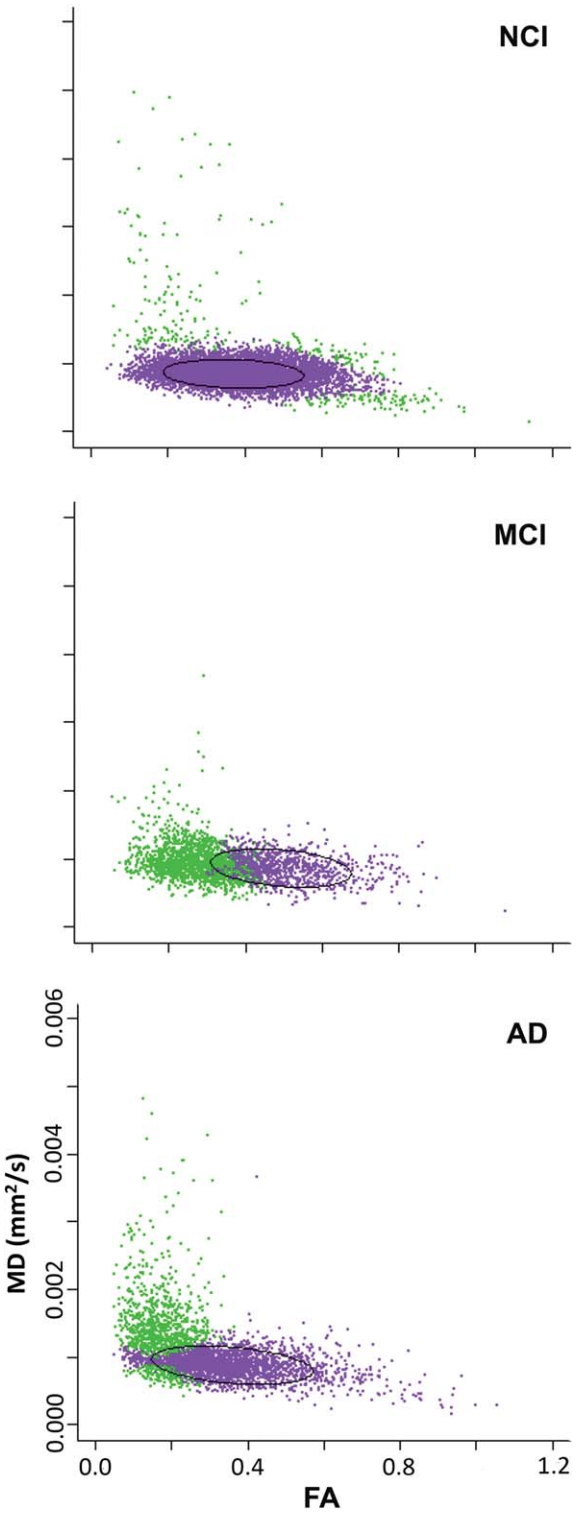

Figure 6. Graphic representation of clusters in the FA/MD space. **Upper panel** shows the location and size of reference cluster (purple) modeled in the NCI group, the **middle panel** in the MCI group, and the **lower panel** for the AD group. Note the progressive increase in the distance to the reference cluster of the voxels not included in the reference (green dots) in the MCI and the AD groups, shown as a shift toward low FA and high MD values. This distance was used as a surrogate to describe structural disruption with respect to a norm.

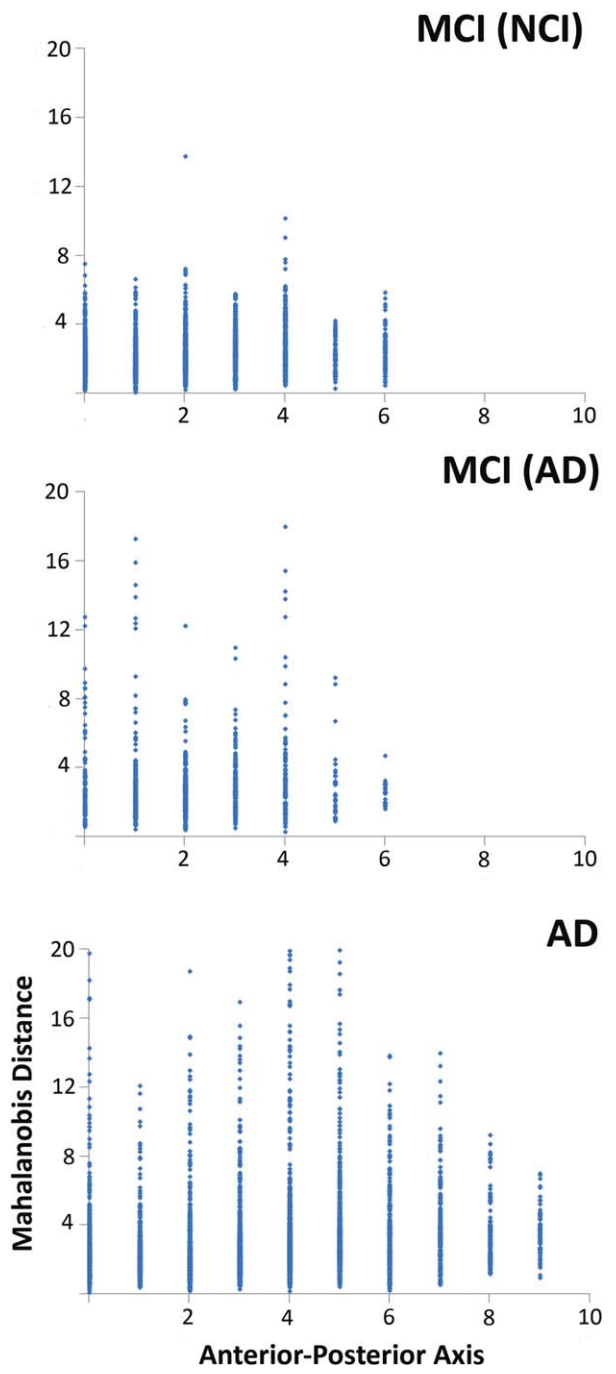

Figure 7. Graphic representation of the distribution of Mahalanobis distances (y axis) on the anatomical space (x axis). Anatomical distribution of distances to the reference cluster shows the predominance of longer values in the anterior portion of the parahippocampal white matter in converted MCI cases (**middle panel**) compared with MCI (NCI) controls (**upper panel**). In comparing the AD cases (**bottom panel**) vs. the converted MCIs, longer distances are seen throughout the whole anterior–posterior extent of the parahippocampal ROI.

voxels per coronal slice) did not depend on the anterior–posterior axis (z coordinate) and did not differ between groups.

DISCUSSION

Changes in the architecture of the parahippocampal white matter as an in vivo biomarker to predict the conversion from MCI to AD

MCI is now an accepted diagnostic category that portends an elevated risk for the development of AD or other dementia (Almkvist et al., 2002; Geslani et al., 2005; Morris, 2005; Petersen, 2004). To improve its predictive potential, several noninvasive imaging-based diagnostic studies that assess structural, metabolic, and functional outcomes associated with conversion of MCI cases to AD have been investigated (for reviews see Baclet-Roussel et al., 2010; Defranceso et al., 2010; McEvoy et al., 2011). However, the specificity of these methods remains inferior to that of invasive neuropathological markers (for reviews see Diniz et al., 2008; Mitchell, 2009; van Rossum et al., 2010). Application of PET-based amyloid imaging may have great diagnostic potential in this regard, but its predictive capacity is limited by the poor correlation of amyloid with disease onset and progression (Chubb et al., 2006; Duyckaerts et al., 2009; Giannakopoulos et al., 2003; Van Hoesen and Solodkin, 1994) and the high cost of these studies compared with MRI.

DTI MRI has emerged as a sensitive method for resolving changes in the structure of neuronal fiber bundles within the brain, and it has been applied to the study of several neurological diseases (Kunimatsu et al., 2003; Mori et al., 2002), including AD (for review see Ewers et al., 2011; Gold et al., 2012; Matthews et al., 2013). We reasoned that its specific application to the early diagnosis, or even prediction of development, of AD would depend on assessing a brain region that displays the earliest pathology. Several studies have shown that the distribution of pathology in AD is not random (Arnold et al., 1991; Nagy et al., 1999; Sassin et al., 2000), and this has been supported by numerous MRI-based studies (Fox and Schott, 2004; Jack et al., 2004; Kantarci et al., 2005). It is precisely this differential distribution of neuronal death in AD (Mitchell et al., 2002) that has led many to apply noninvasive techniques to diagnose early or "prodromal" states of AD (Drago et al., 2011; Killiany et al., 2000; Mortimer and Petersen, 2008; Valls-Pedret et al., 2010).

Although the current sample size that we report is rather small, the clear segregation among our experimental groups suggests that DTI metrics of the parahippocampal white matter region can be a sensitive method to discriminate subjects with AD from cognitively intact subjects. Furthermore, the metric abnormalities were limited to the parahippocampal region and were not present in the corticospinal pathway (Rose et al., 2000), suggesting a selective pathway alteration, at least in earlier disease stages.

It has been reported that NFT pathology within the entorhinal cortex may be present prior to behavioral manifestations of AD (Braak and Braak, 1997a; Mitchell et al., 2002). In this context, our results for MCI subjects were quite interesting. When subjected to discriminant analysis, the four DTI metrics of the parahippocampal white matter region of three of eight (38%) MCI subjects indicated that they belonged to the AD group and five (72%) to the NCI group. At a 1-year followup visit, those MCI subjects classified as AD-like by DTI were reclassified as early AD by clinicians blinded to the imaging data. This correlates well with the prediction that 10–40% of patients diagnosed with MCI convert to AD within 1–2 years (Buchanan, 2009; Falini et al., 2005; Mosconi, 2005; Pavlovic and Pavlovic, 2009; Pennanen et al., 2005). Future studies with larger samples, however, are needed to confirm these preliminary results.

Complex architecture of the parahippocampal ROI

We performed a voxelwise analysis to understand better the potential biological interpretations of the changes observed. For this, we have to consider first the nature of the ROI (parahippocampal white matter).

Although our ROI included the perforant pathway, as with most pathways within the CNS, it is not distinctly segregated. Indeed, although the perforant pathway is the largest cortical association pathway in the temporal lobe (Van Hoesen, 1982, 1995) and its axons form a compact bundle (angular bundle) on their way to the hippocampus, partial volume effects in MR imaging resulting from crossing fibers are common. Because the entorhinal region is a true anatomical hub in the sense of the distributed nature of its connectivity (Insausti et al., 1987a,b; Van Hoesen, 1995), few DTI studies with sophisticated techniques have succeeded in tracking the human perforant path either in vivo or ex vivo (Augustinack et al., 2010; Yassa et al., 2010; Zeineh et al., 2012).

The complex composition of the parahippocampal white matter considered in this study includes connectivity with a large variety of cortical and subcortical regions (e.g., amygdala and limbic thalamus; Amaral and Cowan, 1980; Amaral and Price, 1984) in addition to the reciprocal connections with the hippocampus proper and the subiculum (Rosene and Van Hoesen, 1977; Van Hoesen and Pandya, 1975; Witter, 2007). Indeed, major reciprocal connections of the entorhinal/perirhinal areas originate in cortical association and limbic cortices, including the anterior insula; superior

temporal sulcus; inferior, medial temporal and occipitotemporal regions; anterior and posterior cingulate, peristriate, and orbitofrontal cortices (for review see Insausti, 1993; Lavenex et al., 2002; Van Hoesen, 1995). This multipathway structure necessarily implies that changes captured by DTI metrics will depend on a complex reorganization of the architecture resulting from partial damage to some but not all axons found within the ROI at different times.

AD decreases the complexity of the parahippocampal white matter architecture

The first change we detected in the group and the voxelwise analyses was a decrease of FA in both MCI (AD) and AD individuals as has been reported amply for AD (Ewers et al., 2011; Fellgiebel and Yakushev, 2011; Gold et al., 2012; Matthews et al., 2013; Oishi et al., 2011; Sexton et al., 2010; Stebbins and Murphy, 2009; Stepan-Buksakowska et al., 2012). Because FA is a normalized metric, it does not provide information on the cause of the decrease. It could be due to a decrease in axial diffusivity representing a decrease of the larger diffusion value, an increase in the two secondary Eigen values (radial diffusion), or a combination of both. The relevance of exploring with more precision the origins of the changes observed is that each one of these possibilities can be associated with more specific modifications in the architecture of the tissue. To disambiguate this observation, this initial result has to be considered in the context of the other metrics. Our results show that axial, mean, and radial diffusivities tended toward larger values in AD. In addition, multivariate distributions based on FA/MD showed a clear difference, with lower FA and higher MD values in AD.

The question to be addressed is the nature of the structural changes related to the increase in mean diffusivity along an increase in axial diffusivity in AD. More specifically, the DTI acquisition used a rather low value of b ($b = 900$), at a level that has been suggested to represent extracellular diffusion (Assaf and Cohen, 2000). Hence, the more specific question relates to the nature of the structural changes that are diminishing restrictions to the extracellular diffusion of water along with a simultaneous increase in axial diffusivity. Given this, we posit that the increase in MD can be due to an increase in the size of the extracellular space resulting from degeneration of axonal processes, demyelination, or thinning, in some but not all axons included in the white matter ROI. This increase in the extracellular space can produce a decrease in the degree of crossing fibers within the region, producing an apparent increase in axial diffusivity from the axons less affected by the illness. In other words, our results may reflect a decrease in the complexity of the anatomical architecture of this region reflecting selective and sequential deterioration or structure of limbic and nonlimbic connectivity associated with the parahippocampal region.

Disease progression from MCI to AD is detected by voxel structural disruption

Distances measured from the reference cluster reflect a hierarchical progression shift to lower FA and higher MD-RD values from NCI to MCI (AD) to AD. That is, disease progression involves not only voxels with larger structural changes but also a larger number of them. In other words, even though all subjects (including healthy controls) have voxels with high FA and low MD-RD (voxels within the reference cluster) and voxels with low FA and high MD-RD (damaged voxels), a critical issue may be the relative proportion of these two types of voxels. Is there an inflexion point at which the damaged voxels are at a level in which function is finally compromised?

Distribution of structurally disrupted voxels progresses in an anterior–posterior fashion along the clinical progression of disease

Structurally disrupted voxels were not distributed homogeneously in the parahippocampal white matter of MCI (AD) and AD. Whereas the anterior portion of the parahippocampal white matter had the largest burden of these voxels in MCI patients who converted to AD, in AD these were distributed along the entire rostrocaudal extent of the ROI. The differential distribution of pathological voxels in the anterior parahippocampal region may explain the variance of the probability values associated with MCI membership (to AD or NCI) via discriminant analysis (range 52–100%). In other words, it is possible that focusing the analysis on the anterior regions could increase the sensitivity of the approach.

On the other hand, these regional differences might not be surprising, based on the topology of corticocortical connectivity to and from the entorhinal region in macaques. To illustrate this point, Mohedano-Moriano and colleagues (2007) showed that some of the input connectivity has biases to restricted entorhinal regions. For instance, anterior regions preferentially receive inputs from lateral orbitofrontal regions, anterior cingulate, agranular insula, and visual association cortices. Connectivity to intermediate regions comes from the upper bank of the superior temporal sulcus and auditory association cortices. Finally, posterior regions receive inputs from the parietal and retrosplenial regions. In parallel, the perforant pathway projects to

the hippocampus with an anterior–posterior topology. These three anterior–posterior bands are reminiscent not only of the cytoarchitectural subfields of Amaral, Insausti, and colleagues (Amaral et al., 1987; Insausrti et al., 1995) but also of the organization of the entorhinal intrinsic connectivity (Chrobak and Amaral, 2007). Our results placing the initial changes in the anterior portion of the parahippocampal white matter are consistent with recent DTI reports highlighting early Alzheimer's pathology in limbic regions (Acosta-Cabronero et al., 2010), including its preponderance in anterior hippocampus (Fellgiebel and Yakushev, 2011). Additionally, the fact that pathology extends caudally at later stages of disease suggests that DTI metrics within the parahippocampal white matter can be applied not only as a biomarker for the detection of prodromal AD but also to aid in following the progression of disease into later stages.

Furthermore, we submit that our biomarker for prediction of conversion from MCI to AD might have higher sensitivity by focusing the assessment on the anterior half of the parahippocampal white matter. We have preliminary data suggesting that the distribution of damaged voxels might also have a bias to the medial portion of this region. Confirmation of this preliminary observation, however, awaits further analysis.

ACKNOWLEDGMENTS

We thank Gina Freed, RN, for her valuable assistance in recruiting volunteers; Mr. Robert Lyons for technical help in performing the scan sessions; Dr. M. Lacy for assisting with the neuropsychological testing; and Drs. D. Traub and S.L. Small for their editorial comments.

CONFLICT OF INTEREST STATEMENT

The authors report no conflicts of interest.

ROLE OF AUTHORS

All authors had full access to all the data in the study and take responsibility for the integrity of the data and the accuracy of the data analysis. Study concept and design: ASo, JM, GWVH, LH. Acquisition of data: ASo, JM. Analysis and interpretation of data: ASo, JM, EEC, LH, GWVH, FK, ASh. Drafting of the manuscript: ASo, JM, FK. Critical revision of the manuscript for important intellectual content: ASo, JM, FK. Statistical analysis: EEC, FK. Obtained funding: ASo. Study supervision: ASo, JM.

LITERATURE CITED

Acosta-Cabronero J, Williams GB, Pengas G, Nestor PJ. 2010. Absolute diffusivities define the landscape of white matter degeneration in Alzheimer's disease. Brain 133:529–539.

Albert MS, DeKosky ST, Dickson D, Dubois B, Feldman HH, Fox NC, Gamst A, Holtzman DM, Jagust WJ, Petersen RC, Snyder PJ, Carrillo MC, Thies B, Phelps CH. 2011. The diagnosis of mild cognitive impairment due to Alzheimer's disease: recommendations from the National Institute on Aging–Alzheimer's Association workgroups on diagnostic guidelines for Alzheimer's disease. Alzheimers Dement 7:270–279.

Almkvist O, Axelman K, Basun H, Wahlund LO, Lannfelt L. 2002. Conversion from preclinical to dinical stage of Alzheimer's disease as shown by decline of cognitive function in carriers of the Swedish APP-mutation. J Neural Transmiss Suppl, 117–125.

Amaral DG, Cowan WM. 1980. Subcortical afferents to the hippocampal formation in the monkey. J Comp Neurol 189:573–591.

Amaral DG, Price JL. 1984. Amygdalo-cortical projections in the monkey (*Macaca fascicularis*). J Comp Neurol 230: 465–496.

Amaral DG, Insausti R, Cowan WM. 1987. The entorhinal cortex of the monkey: I. Cytoarchitectonic organization. J Comp Neurol 264:326–355.

Arenaza-Urquijo EM, Bosch B, Sala-Llonch R, Sole-Padulles C, Junque C, Fernandez-Espejo D, Bargallo N, Rami L, Molinuevo JL, Bartres-Faz D. 2010. Specific anatomic associations between white matter integrity and cognitive reserve in normal and cognitively impaired elders. Am J Geriatr Psychiatry 19:33–42.

Arnold SE, Hyman BT, Flory J, Damasio AR, van Hoesen GW. 1991. The topographical and neuroanatomical distribution of neurofibrillary tangles and neuritic plaques in the cerebral cortex of patients with Alzheimer's disease. Cereb Cortex 1:103–116.

Assaf Y, Cohen Y. 2000. Assignment of the water slow-diffusing component in the central nervous system using q-space diffusion MRS: implications for fiber tract imaging. Magn Reson Med 43:191–199.

Augustinack JC, Helmer K, Huber KE, Kakunoori S, Zollei L, Fischl B. 2010. Direct visualization of the perforant pathway in the human brain with ex vivo diffusion tensor imaging. Front Hum Neurosci 4:42.

Baclet-Roussel C, Ankri J, Ergis AM. 2010. [Contribution of various MRI techniques to the characterization of mild cognitive impairment]. Psychol Neuropsychiatr Vieil 8: 53–64.

Basser PJ, Pierpaoli C. 1996. Microstructural and physiological features of tissues elucidated by quantitative-diffusion-tensor MRI. J Magn Reson B 111:209–219.

Behrens TE, Woolrich MW, Jenkinson M, Johansen-Berg H, Nunes RG, Clare S, Matthews PM, Brady JM, Smith SM. 2003. Characterization and propagation of uncertainty in diffusion-weighted MR imaging. Magn Reson Med 50: 1077–1088.

Benedict RHB, Schretlen D, Groniger L, Dobraski M, Shpritz B. 1996. Revision of the brief Visuospatial Memory test: studies of normal performance, reliability, and validity. Psychol Assess 8:145–153.

Bosch B, Arenaza-Urquijo EM, Rami L, Sala-Llonch R, Junque C, Sole-Padulles C, Pena-Gomez C, Bargallo N, Molinuevo JL, Bartres-Faz D. 2010. Multiple DTI index analysis in normal aging, amnestic MCI and AD. Relationship with neuropsychological performance. Neurobiol Aging 33:61–74.

Braak H, Braak E. 1997a. Frequency of stages of Alzheimer-related lesions in different age categories. Neurobiol Aging 18:351–357.

Braak H, Braak E. 1997b. Staging of Alzheimer-related cortical destruction. Int Psychogeriatry 9(Suppl 1):257–261; discussion 269–272.

Braskie MN, Klunder AD, Hayashi KM, Protas H, Kepe V, Miller KJ, Huang SC, Barrio JR, Ercoli LM, Siddarth P, Satyamurthy N, Liu J, Toga AW, Bookheimer SY, Small GW, Thompson PM. 2010. Plaque and tangle imaging and cognition in normal aging and Alzheimer's disease. Neurobiol Aging 31:1669–1678.

Buchanan D. 2009. Review: long-term annual conversion rate to dementia was 3.3% in elderly people with mild cognitive impairment. Evidence-Based Nursing 12:87.

Butts T, Chaplin N, Wingate RJ. 2011. Can clues from evolution unlock the molecular development of the cerebellum? Mol Neurobiol 43:67–76.

Chen TF, Lin CC, Chen YF, Liu HM, Hua MS, Huang YC, Chiu MJ. 2009. Diffusion tensor changes in patients with amnesic mild cognitive impairment and various dementias. Psychiatr Res 173:15–21.

Cherubini A, Peran P, Spoletini I, Di Paola M, Di Iulio F, Hagberg GE, Sancesario G, Gianni W, Bossu P, Caltagirone C, Sabatini U, Spalletta G. 2010. Combined volumetry and DTI in subcortical structures of mild cognitive impairment and Alzheimer's disease patients. J Alzheimers Dis 19:1273–1282.

Chetelat G, Eustache F, Viader F, De La Sayette V, Pelerin A, Mezenge F, Hannequin D, Dupuy B, Baron JC, Desgranges B. 2005. FDG-PET measurement is more accurate than neuropsychological assessments to predict global cognitive deterioration in patients with mild cognitive impairment. Neurocase 11:14–25.

Chrobak JJ, Amaral DG. 2007. Entorhinal cortex of the monkey: VII. Intrinsic connections. J Comp Neurol 500:612–633.

Chubb C, Inagaki Y, Sheu P, Cummings B, Wasserman A, Head E, Cotman C. 2006. BioVision: an application for the automated image analysis of histological sections. Neurobiol Aging 27:1462–1476.

Clark CM, Pontecorvo MJ, Beach TG, Bedell BJ, Coleman RE, Doraiswamy PM, Fleisher AS, Reiman EM, Sabbagh MN, Sadowsky CH, Schneider JA, Arora A, Carpenter AP, Flitter ML, Joshi AD, Krautkramer MJ, Lu M, Mintun MA, Skovronsky DM, Group A-AS. 2012. Cerebral PET with florbetapir compared with neuropathology at autopsy for detection of neuritic amyloid-beta plaques: a prospective cohort study. Lancet Neurol 11:669–678.

Damoiseaux JS, Smith SM, Witter MP, Sanz-Arigita EJ, Barkhof F, Scheltens P, Stam CJ, Zarei M, Rombouts SA. 2009. White matter tract integrity in aging and Alzheimer's disease. Hum Brain Mapp 30:1051–1059.

Davatzikos C, Xu F, An Y, Fan Y, Resnick SM. 2009. Longitudinal progression of Alzheimer's-like patterns of atrophy in normal older adults: the SPARE-AD index. Brain 132: 2026–2035.

Davatzikos C, Bhatt P, Shaw LM, Batmanghelich KN, Trojanowski JQ. 2010. Prediction of MCI to AD conversion, via MRI, CSF biomarkers, and pattern classification. Neurobiol Aging 32:19–27.

de Crespigny AJ, Marks MP, Enzmann DR, Moseley ME. 1995. Navigated diffusion imaging of normal and ischemic human brain. Magn Reson Imaging 33:720–728.

De Toledo-Morrell L, Goncharova I, Dickerson B, Wilson RS, Bennett DA. 2000. From healthy aging to early Alzheimer's disease: in vivo detection of entorhinal cortex atrophy. Ann N Y Acad Sci 911:240–253.

Defranceso M, Schocke M, Messner HJ, Deisenhammer EA, Hinterhuber H, Marksteiner J, Weiss EM. 2010. [Conversion from MCI (mild cognitive impairment) to Alzheimer's disease: diagnostic options and predictors]. Neuropsychiatry 24:88–98.

Dejerine J, Dejerine-Klumpke M. 1901. Anatomie des centres nerveux. Anatomie du cerveau—anatomie du rhombencephale. Paris: J. Rueff, Editeur.

Diniz BS, Pinto Junior JA, Forlenza OV. 2008. Do CSF total tau, phosphorylated tau, and beta-amyloid 42 help to predict progression of mild cognitive impairment to Alzheimer's disease? A systematic review and meta-analysis of the literature. World J Biol Psychiatry 9:172–182.

Drago V, Babiloni C, Bartres-Faz D, Caroli A, Bosch B, Hensch T, Didic M, Klafki HW, Pievani M, Jovicich J, Venturi L, Spitzer P, Vecchio F, Schoenknecht P, Wiltfang J, Redolfi A, Forloni G, Blin O, Irving E, Davis C, Hardemark HG, Frisoni GB. 2011. Disease tracking markers for Alzheimer's disease at the prodromal (MCI) stage. J Alzheimers Dis 26 Suppl 3:159–199.

Driscoll I, Troncoso JC, Rudow G, Sojkova J, Pletnikova O, Zhou Y, Kraut MA, Ferrucci L, Mathis CA, Klunk WE, O'Brien RJ, Davatzikos C, Wong DF, Resnick SM. 2012. Correspondence between in vivo ^{11}C-PiB-PET amyloid imaging and postmortem, region-matched assessment of plaques. Acta Neuropathol 124:823–831.

Duvernoy HM. 1988. The human hippocampus: an atlas of applied anatomy. Munchen: J.F. Bergmann Verlag.

Duyckaerts C, Delatour B, Potier MC. 2009. Classification and basic pathology of Alzheimer disease. Acta Neuropathol 118:5–36.

Ewers M, Frisoni GB, Teipel SJ, Grinberg LT, Amaro E Jr, Heinsen H, Thompson PM, Hampel H. 2011. Staging Alzheimer's disease progression with multimodality neuroimaging. Prog Neurobiol 95:535–546.

Falini A, Bozzali M, Magnani G, Pero G, Gambini A, Benedetti B, Mossini R, Franceschi M, Comi G, Scotti G, Filippi M. 2005. A whole brain MR spectroscopy study from patients with Alzheimer's disease and mild cognitive impairment. Neuroimage 26:1159–1163.

Fellgiebel A, Yakushev I. 2011. Diffusion tensor imaging of the hippocampus in MCI and early Alzheimer's disease. J Alzheimers Dis 26(Suppl 3):257–262.

Fellgiebel A, Wille P, Muller MJ, Winterer G, Scheurich A, Vucurevic G, Schmidt LG, Stoeter P. 2004. Ultrastructural hippocampal and white matter alterations in mild cognitive impairment: a diffusion tensor imaging study. Dement Geriatr Cogn Disord 18:101–108.

Fellgiebel A, Dellani PR, Greverus D, Scheurich A, Stoeter P, Muller MJ. 2006. Predicting conversion to dementia in mild cognitive impairment by volumetric and diffusivity measurements of the hippocampus. Psychiatr Res 146: 283–287.

Filler AG, Bell BA. 1992. Axonal transport, imaging, and the diagnosis of nerve compression. Br J Neurosurg 6:293–295.

Fischer P, Jungwirth S, Zehetmayer S, Weissgram S, Hoenigschnabl S, Gelpi E, Krampla W, Tragl KH. 2007. Conversion from subtypes of mild cognitive impairment to Alzheimer dementia. Neurology 68:288–291.

Fox NC, Schott JM. 2004. Imaging cerebral atrophy: normal ageing to Alzheimer's disease. Lancet 363:392–394.

Fraley C, Raftery AE. 2007. Model-based methods of classification: using the mclust software in cehmometrics. J Statist Software 18(6).

Furumoto S, Okamura N, Furukawa K, Tashiro M, Ishikawa Y, Sugi K, Tomita N, Waragai M, Harada R, Tago T, Iwata R, Yanai K, Arai H, Kudo Y. 2013. A ^{18}F-labeled BF-227 derivative as a potential radioligand for imaging dense amyloid plaques by positron emission tomography. Mol Imaging Biol (in press).

Geslani DM, Tierney MC, Herrmann N, Szalai JP. 2005. Mild cognitive impairment: an operational definition and its conversion rate to Alzheimer's disease. Dement Geriatr Cogn Disord 19:383–389.

Giannakopoulos P, Herrmann FR, Bussiere T, Bouras C, Kovari E, Perl DP, Morrison JH, Gold G, Hof PR. 2003. Tangle and neuron numbers, but not amyloid load, predict cognitive status in Alzheimer's disease. Neurology 60:1495–1500.

Gold BT, Johnson NF, Powell DK, Smith CD. 2012. White matter integrity and vulnerability to Alzheimer's disease: preliminary findings and future directions. Biochim Biophys Acta 1822:416–422.

Gomez-Isla T, Price JL, McKeel DW Jr, Morris JC, Growdon JH, Hyman BT. 1996. Profound loss of layer II entorhinal cortex neurons occurs in very mild Alzheimer's disease. J Neurosci 16:4491–4500.

Gomez-Isla T, Spires T, De Calignon A, Hyman BT. 2008. Neuropathology of Alzheimer's disease. Hdbk Clin Neurol 89: 233–243.

Hampel H, Burger K, Teipel SJ, Bokde AL, Zetterberg H, Blennow K. 2008. Core candidate neurochemical and imaging biomarkers of Alzheimer's disease. Alzheimers Dement 4:38–48.

Insausti R. 1993. Comparative anatomy of the entorhinal cortex and hippocampus in mammals. Hippocampus 3(Spec. No.):19–26.

Insausti R, Amaral DG, Cowan WM. 1987a. The entorhinal cortex of the monkey: II. Cortical afferents. J Comp Neurol 264:356–395.

Insausti R, Amaral DG, Cowan WM. 1987b. The entorhinal cortex of the monkey: III. Subcortical afferents. J Comp Neurol 264:396–408.

Insausti R, Tunon T, Sobreviela T, Insausti AM, Gonzalo LM. 1995. The human entorhinal cortex: a cytoarchitectonic analysis. J Comp Neurol 355:171–198.

Jack CR Jr, Shiung MM, Gunter JL, O'Brien PC, Weigand SD, Knopman DS, Boeve BF, Ivnik RJ, Smith GE, Cha RH, Tangalos EG, Petersen RC. 2004. Comparison of different MRI brain atrophy rate measures with clinical disease progression in AD. Neurology 62:591–600.

Jack CR Jr, Bernstein MA, Borowski BJ, Gunter JL, Fox NC, Thompson PM, Schuff N, Krueger G, Killiany RJ, Decarli CS, Dale AM, Carmichael OW, Tosun D, Weiner MW. 2010. Update on the magnetic resonance imaging core of the Alzheimer's disease neuroimaging initiative. Alzheimers Dement 6:212–220.

Jensen JR, Cisek K, Funk KE, Naphade S, Schafer KN, Kuret J. 2011. Research towards tau imaging. J Alzheimers Dis 26(Suppl 3):147–157.

Kalus P, Slotboom J, Gallinat J, Mahlberg R, Cattapan-Ludewig K, Wiest R, Nyffeler T, Buri C, Federspiel A, Kunz D, Schroth G, Kiefer C. 2006. Examining the gateway to the limbic system with diffusion tensor imaging: the perforant pathway in dementia. Neuroimage 30:713–720.

Kantarci K, Petersen RC, Boeve BF, Knopman DS, Weigand SD, O'Brien PC, Shiung MM, Smith GE, Ivnik RJ, Tangalos EG, Jack CR Jr. 2005. DWI predicts future progression to Alzheimer disease in amnestic mild cognitive impairment. Neurology 64:902–904.

Kaplan E, Goodglass J, Weintraub S. 1983. Boston Naming Test. Philadelphia: Lea and Febiger.

Killiany RJ, Gomez-Isla T, Moss M, Kikinis R, Sandor T, Jolesz F, Tanzi R, Jones K, Hyman BT, Albert MS. 2000. Use of structural magnetic resonance imaging to predict who will get Alzheimer's disease. Ann Neurol 47:430–439.

Kunimatsu A, Aoki S, Masutani Y, Abe O, Mori H, Ohtomo K. 2003. Three-dimensional white matter tractography by diffusion tensor imaging in ischaemic stroke involving the corticospinal tract. Neuroradiology 45:532–535.

Lavenex P, Suzuki WA, Amaral DG. 2002. Perirhinal and parahippocampal cortices of the macaque monkey: projections to the neocortex. J Comp Neurol 447:394–420.

Le Bihan D, Mangin JF, Poupon C, Clark CA, Pappata S, Molko N, Chabriat H. 2001. Diffusion tensor imaging: concepts and applications. J Magn Reson Imaging 13:534–546.

Lehrner J, Gufler R, Guttmann G, Maly J, Gleiss A, Auff E, DalBianco P. 2005. Annual conversion to Alzheimer'sdisease among patients with memory complaints attending an outpatient memory clinic: the influence of amnestic mild cognitive impairment and the predictive value of neuropsychological testing. Wien Klin Wochenschrift 117:629–635.

Liu Y, Spulber G, Lehtimaki KK, Kononen M, Hallikainen I, Grohn H, Kivipelto M, Hallikainen M, Vanninen R, Soininen H. 2009. Diffusion tensor imaging and tract-based spatial statistics in Alzheimer's disease and mild cognitive impairment. Neurobiol Aging.

Matthews PM, Filippini N, Douaud G. 2013. Brain structural and functional connectivity and the progression of neuropathology in Alzheimer's disease. J Alzheimers Dis 33(Suppl 1):S163–S172.

McEvoy LK, Holland D, Hagler DJ Jr, Fennema-Notestine C, Brewer JB, Dale AM,Alzheimer's Disease Neuroimaging. 2011. Mild cognitive impairment: baseline and longitudinal structural MR imaging measures improve predictive prognosis. Radiology 259:834–843.

McKhann GM, Knopman DS, Chertkow H, Hyman BT, Jack CR Jr, Kawas CH, Klunk WE, Koroshetz WJ, Manly JJ, Mayeux R, Mohs RC, Morris JC, Rossor MN, Scheltens P, Carrillo MC, Thies B, Weintraub S, Phelps CH. 2011. The diagnosis of dementia due to Alzheimer's disease: recommendations from the National Institute on Aging-Alzheimer's Association workgroups on diagnostic guidelines for Alzheimer's disease. Alzheimers Dement 7:263–269.

Misra C, Fan Y, Davatzikos C. 2009. Baseline and longitudinal patterns of brain atrophy in MCI patients, and their use in prediction of short-term conversion to AD: results from ADNI. Neuroimage 44:1415–1422.

Mitchell AJ. 2009. CSF phosphorylated tau in the diagnosis and prognosis of mild cognitive impairment and Alzheimer's disease: a meta-analysis of 51 studies. J Neurol Neurosurg Psychiatry 80:966–975.

Mitchell TW, Mufson EJ, Schneider JA, Cochran EJ, Nissanov J, Han LY, Bienias JL, Lee VM, Trojanowski JQ, Bennett DA, Arnold SE. 2002. Parahippocampal tau pathology in healthy aging, mild cognitive impairment, and early Alzheimer's disease. Ann Neurol 51:182–189.

Modrego PJ. 2006. Predictors of conversion to dementia of probable Alzheimer type in patients with mild cognitive impairment. Curr Alzheimer Res 3:161–170.

Mohedano-Moriano A, Pro-Sistiaga P, Arroyo-Jimenez MM, Artacho-Perula E, Insausti AM, Marcos P, Cebada-Sanchez S, Martinez-Ruiz J, Munoz M, Blaizot X, Martinez-Marcos A, Amaral DG, Insausti R. 2007. Topographical and laminar distribution of cortical input to the monkey entorhinal cortex. J Anat 211:250–260.

Mori S, Frederiksen K, van Zijl PC, Stieltjes B, Kraut MA, Solaiyappan M, Pomper MG. 2002. Brain white matter anatomy of tumor patients evaluated with diffusion tensor imaging. Ann Neurol 51:377–380.

Morris JC. 2005. Mild cognitive impairment and preclinical Alzheimer's disease. Geriatrics Suppl:9–14.

Mortimer JA, Petersen RC. 2008. Detection of prodromal Alzheimer's disease. Ann Neurol 64:479–480.

Mosconi L. 2005. Brain glucose metabolism in the early and specific diagnosis of Alzheimer's disease. FDG-PET studies in MCI and AD. Eur J Nucl Med Mol Imaging 32:486–510.

Muller MJ, Greverus D, Dellani PR, Weibrich C, Wille PR, Scheurich A, Stoeter P, Fellgiebel A. 2005. Functional implications of hippocampal volume and diffusivity in mild cognitive impairment. Neuroimage 28:1033–1042.

Nagy Z, Hindley NJ, Braak H, Braak E, Yilmazer-Hanke DM, Schultz C, Barnetson L, King EM, Jobst KA, Smith AD. 1999. The progression of Alzheimer's disease from limbic regions to the neocortex: clinical, radiological and pathological relationships. Dement Geriatr Cogn Disord 10: 115–120.

Oishi K, Mielke MM, Albert M, Lyketsos CG, Mori S. 2011. DTI analyses and clinical applications in Alzheimer's disease. J Alzheimers Dis 26(Suppl 3):287–296.

Okamura N, Yanai K. 2010. Florbetapir ^{18}F, a PET imaging agent that binds to amyloid plaques for the potential detection of Alzheimer's disease. IDrugs 13:890–899.

Ono M. 2009. Development of positron-emission tomography/single-photon emission computed tomography imaging probes for in vivo detection of beta-amyloid plaques in Alzheimer's brains. Chem Pharm Bull (Tokyo) 57:1029–1039.

Pavlovic DM, Pavlovic AM. 2009. [Mild cognitive impairment]. Srp Arh Celok Lek 137:434–439.

Pennanen C, Testa C, Laakso MP, Hallikainen M, Helkala EL, Hanninen T, Kivipelto M, Kononen M, Nissinen A, Tervo S, Vanhanen M, Vanninen R, Frisoni GB, Soininen H. 2005. A voxel based morphometry study on mild cognitive impairment. J Neurol Neurosurg Psychiatry 76:11–14.

Petersen RC. 2004. Mild cognitive impairment as a diagnostic entity. J Intern Med 256:183–194.

Petersen RC, Negash S. 2008. Mild cognitive impairment: an overview. CNS Spectr 13:45–53.

Pierpaoli C, Jezzard P, Basser PJ, Barnett A, Di Chiro G. 1996. Diffusion tensor MR imaging of the human brain. Radiology 201:637–648.

Reitan RM. 1958. Validity of the Trail Making Test as an indication of organic brain damage. Percept Mot Skills 8: 271–276.

Rogalski EJ, Murphy CM, deToledo-Morrell L, Shah RC, Moseley ME, Bammer R, Stebbins GT. 2009. Changes in parahippocampal white matter integrity in amnestic mild cognitive impairment: a diffusion tensor imaging study. Behav Neurol 21:51–61.

Rose SE, Chen F, Chalk JB, Zelaya FO, Strugnell WE, Benson M, Semple J, Doddrell DM. 2000. Loss of connectivity in Alzheimer's disease: an evaluation of white matter tract integrity with colour coded MR diffusion tensor imaging. J Neurol Neurosurg Psychiatry 69:528–530.

Rose SE, McMahon KL, Janke AL, O'Dowd B, de Zubicaray G, Strudwick MW, Chalk JB. 2006. Diffusion indices on magnetic resonance imaging and neuropsychological performance in amnestic mild cognitive impairment. J Neurol Neurosurg Psychiatry 77:1122–1128.

Rosene DL, Van Hoesen GW. 1977. Hippocampal efferents reach widespread areas of cerebral cortex and amygdala in the rhesus monkey. Science 198:315–317.

Sassin I, Schultz C, Thal DR, Rub U, Arai K, Braak E, Braak H. 2000. Evolution of Alzheimer's disease-related cytoskeletal changes in the basal nucleus of Meynert. Acta Neuropathol 100:259–269.

Schwarz G. 1978. Estimating the dimensions of a model. Ann Statist 6:461–464.

Sexton CE, Kalu UG, Filippini N, Mackay CE, Ebmeier KP. 2010. A meta-analysis of diffusion tensor imaging in mild cognitive impairment and Alzheimer's disease. Neurobiol Aging 32:5–18.

Shapiro AM, Benedict RH, Schretlen D, Brandt J. 1999. Construct and concurrent validity of the Hopkins Verbal Learning Test revised. Clin Neuropsychol 13:348–358.

Shin J, Kepe V, Barrio JR, Small GW. 2011. The merits of FDDNP-PET imaging in Alzheimer's disease. J Alzheimers Dis 26(Suppl 3):135–145.

Small GW. 2002. Brain-imaging surrogate markers for detection and prevention of age-related memory loss. J Mol Neurosci 19:17–21.

Small GW, Agdeppa ED, Kepe V, Satyamurthy N, Huang SC, Barrio JR. 2002. In vivo brain imaging of tangle burden in humans. J Mol Neurosci 19:323–327.

Solodkin A, Hlustik P, Chen EE, Small SL. 2004. Fine modulation in network activation during motor execution and motor imagery. Cereb Cortex 14:1246–1255.

Spreen O, Strauss E. 1998. Controlled oral word association. A compendium of neuropsychological tests, 2nd ed. New York: Oxford University Press. p 447–464.

Sprooten E, Lymer GK, Munoz Maniega S, McKirdy J, Clayden JD, Bastin ME, Porteous D, Johnstone EC, Lawrie SM, Hall J, McIntosh AM. 2009. The relationship of anterior thalamic radiation integrity to psychosis risk associated neuregulin-1 variants. Mol Psychiatry 14:237–238, 233.

Stebbins GT, Murphy CM. 2009. Diffusion tensor imaging in Alzheimer's disease and mild cognitive impairment. Behav Neurol 21:39–49.

Stenset V, Bjornerud A, Fjell AM, Walhovd KB, Hofoss D, Due-Tonnessen P, Gjerstad L, Fladby T. 2009. Cingulum fiber diffusivity and CSF T-tau in patients with subjective and mild cognitive impairment. Neurobiol Aging 32:581–589.

Stepan-Buksakowska I, Keller J, Laczo J, Rulseh A, Hort J, Lisy J, Charvat F, Rocek M, Horinek D. 2012. Diffusion tensor imaging in Alzheimer disease and mild cognitive impairment. Neurol Neurochir Pol 46:462–471.

Suva D, Favre I, Kraftsik R, Esteban M, Lobrinus A, Miklossy J. 1999. Primary motor cortex involvement in Alzheimer disease. J Neuropathol Exp Neurol 58:1125–1134.

Teipel SJ, Meindl T, Wagner M, Stieltjes B, Reuter S, Hauenstein KH, Filippi M, Ernemann U, Reiser MF, Hampel H. 2010. Longitudinal changes in fiber tract integrity in healthy aging and mild cognitive impairment: a DTI follow-up study. J Alzheimers Dis 22:507–522.

Trojanowski JQ. 2002. Tauists, Baptists, Syners, Apostates, and new data. Ann Neurol 52:263–265.

Valls-Pedret C, Molinuevo JL, Rami L. 2010. [Early diagnosis of Alzheimer's disease: the prodromal and preclinical phase]. Rev Neurol 51:471–480.

Van Hoesen GW. 1982. The parahippocampal gyrus: new observations regarding its cortical connections in the monkey. Trends Neurosci 5:345–350.

Van Hoesen GW. 1995. Anatomy of the medial temporal lobe. Magn Reson Imaging 13:1047–1055.

Van Hoesen GW, Pandya DN. 1975. Some connections of the entorhinal (area 28) and perirhinal (area 35) cortices of the rhesus monkey. III. Efferent connections. Brain Res 95:39–59.

Van Hoesen GW, Solodkin A. 1993. Some modular features of temporal cortex in humans as revealed by pathological changes in Alzheimer's disease. Cereb Cortex 3:465–475.

Van Hoesen GW, Solodkin A. 1994. Cellular and system neuroanatomical changes in Alzheimer's disease. Ann N Y Acad Sci 747:12–35.

Van Hoesen GW, Hyman BT, Damasio AR. 1991. Entorhinal cortex pathology in Alzheimer's disease. Hippocampus 1:1–8.

Van Hoesen GW, Augustinack JC, Dierking J, Redman SJ, Thangavel R. 2000. The parahippocampal gyrus in Alzheimer's disease. Clinical and preclinical neuroanatomical correlates. Ann N Y Acad Sci 911:254–274.

van Rossum IA, Vos S, Handels R, Visser PJ. 2010. Biomarkers as predictors for conversion from mild cognitive impairment to Alzheimer-type dementia: implications for trial design. J Alzheimers Dis 20:881–891.

Wilkinson GS. 1993. The Wide Range Achievement Test—III. Wimnington, DE: Jastack Associates, A division of Wide Range Inc.

Wippold FJ 2nd, Cairns N, Vo K, Holtzman DM, Morris JC. 2008. Neuropathology for the neuroradiologist: plaques and tangles. AJNR Am J Neuroradiol 29:18–22.

Witter MP. 2007. The perforant path: projections from the entorhinal cortex to the dentate gyrus. Prog Brain Res 163:43–61.

Woods R, Grafton S, Holmes C, Cherry S, Mazziotta J. 1998. Automated image registration: I. General methods and intrasubject, intramodality validation. J Comput Assist Tomogr 22:141–154.

Yassa MA, Muftuler LT, Stark CE. 2010. Ultrahigh-resolution microstructural diffusion tensor imaging reveals perforant path degradation in aged humans in vivo. Proc Natl Acad Sci U S A 107:12687–12691.

Yesavage JA, Brink TL, Rose TL, Adey M. 1983. The Geriatric Depression Rating Scale: comparison with other self-report and psychiatric rating scales. In: Crook T, editor. Assessment in geriatric psychopharmacology. New Canaan, CT: Mark Powley Associates. p 153–167.

Zeineh MM, Holdsworth S, Skare S, Atlas SW, Bammer R. 2012. Ultra-high resolution diffusion tensor imaging of the microscopic pathways of the medial temporal lobe. Neuroimage 62:2065–2082.